Electrical structure beneath the northern MELT line on the East Pacific Rise at 15°45′S

Kiyoshi Baba,[1] Pascal Tarits,[1,2] Alan D. Chave,[3] Rob L. Evans,[3] Greg Hirth,[3] and Randall L. Mackie[4]

Received 19 July 2006; revised 7 October 2006; accepted 18 October 2006; published 16 November 2006.

[1] The electrical structure of the upper mantle beneath the East Pacific Rise (EPR) at 15°45′S is imaged by inverting seafloor magnetotelluric data obtained during the Mantle ELectromagnetic and Tomography (MELT) experiment. The electrical conductivity model shows no evidence for a conductive region immediately beneath the ridge, in contrast to the model previously obtained beneath the EPR at 17°S. This observation can be explained by differences in current melt production along the ridge, consistent with other observations. The mantle to the east of the ridge at 60 –100 km depth is anisotropic, with higher conductivity in the spreading direction compared to the along-strike direction, similar to the 17°S region. The high conductivity in the spreading direction can be explained by a hydrated mantle with strain-induced lattice preferred orientation of olivine or by partial melt preferentially connected in the spreading direction. **Citation:** Baba, K., P. Tarits, A. D. Chave, R. L. Evans, G. Hirth, and R. L. Mackie (2006), Electrical structure beneath the northern MELT line on the East Pacific Rise at 15°45′S, *Geophys. Res. Lett.*, *33*, L22301, doi:10.1029/2006GL027528.

1. Introduction

[2] The melt generation process beneath mid-ocean ridges provides the key to understanding the creation of new oceanic plates within the framework of plate tectonics. The Mantle ELectromagnetic and Tomography (MELT) experiment imaged a partial melt zone and surrounding structure using marine seismic and electromagnetic (EM) surveys [*MELT Seismic Team*, 1998; *Evans et al.*, 1999]. The experiment targeted the longest ridge segment on the southern East Pacific Rise (EPR) between the Garrett Transform Fault at ~13°30′S and the large overlapping spreading center (OSC) at 20°40′S. Despite the largely two-dimensional (2-D) surface character of the ridge, there are along-axis variations in surface morphology and geophysical or geochemical observables within the ridge segment that are associated with variability in magma supply and chemical heterogeneity [e.g., *Hooft et al.*, 1997; *Kurz et al.*, 2005]. The EM component of the MELT experiment featured two survey lines, crossing the ridge axis at 17°S and 15°45′S, where the ridge crest is wide and inflated (suggesting an abundant magma supply) and narrow and deflated (suggesting a poor magma supply at present), respectively [*Evans et al.*, 1999]. These two survey lines were chosen to look for along-ridge variations in magma supply related to the width of the ridge-axis. The sensitivity of electrical conductivity to interconnected melt, hydrogen dissolved in minerals, and temperature is different than that for seismic velocity, and thus is useful for differentiating the mantle structure in these two regions.

[3] Previous MELT-EM studies focused on the southern line (17°S) along which the data coverage was more extensive [*Evans et al.*, 1999, 2005; *Baba et al.*, 2006]. The key features of these studies are 1) an asymmetric conductive region that is at least 100 km wide and has a greater extent to the west of the ridge, similar to the results from seismic imaging [e.g., *MELT Seismic Team*, 1998; *Dunn and Forsyth*, 2003] – the conductivity in the region suggests melt fractions of about 1 %, 2) a higher mantle conductivity in the spreading direction than along-strike below 60 km off-axis and to the east of the ridge independent of lithospheric age, and 3) a resistive mantle above 60 km depth. The second and third features may be interpreted in terms of mantle hydration in conjunction with the presence of lattice preferred orientation of olivine below 60 km together with an overriding resistive layer that has been dehydrated due to the melting processes associated with plate accretion.

[4] This paper interprets the northern line data from the MELT-EM experiment. A 2-D electrical conductivity model of the upper mantle, that allows anisotropy, is obtained through inversion. The model is compared with that obtained for the EPR at 17°S reported by *Baba et al.* [2006]. We discuss the melt generation process and related mantle dynamics through comparison of the models from each region.

2. Data and Data Analysis

[5] The northern line of the MELT-EM experiment consists of 13 sites (Figure 1) extending 200 km on either side of the rise crest. Usable electric or magnetic field data were recovered from only seven sites. As a result, the data coverage more than 30 km west of the ridge is limited. The electromagnetic field time series were processed using a bounded influence estimator [*Chave and Thomson*, 2004] and six full tensor magnetotelluric (MT) response functions were recovered. The limited available data means that in some instances the MT response function was calculated using a combination of electric and magnetic field data that are not co-located (Table 1). The actual location of the electric and magnetic field measurements was accounted for during modeling and inversion.

[1] Earthquake Research Institute, University of Tokyo, Japan.
[2] UMR CNRS 'Domaines Océaniques', IUEM/UBO, Plouzané, France.
[3] Woods Hole Oceanographic Institution, Woods Hole, Massachusetts, USA.
[4] GSY-USA, Inc., San Francisco, California, USA.

0094-8276/06/2006GL027528$05.00

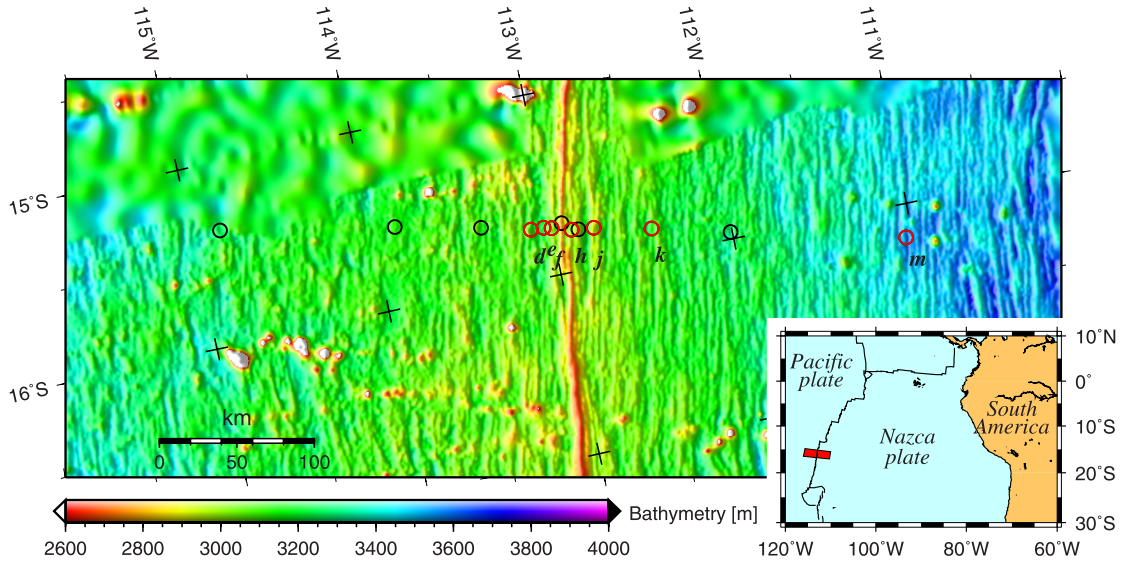

Figure 1. Location of the northern line MELT EM sites superimposed on a bathymetric map. The red circles with labels are the sites where the available data were recovered (see Table 1). The inset shows the location of the experiment (red box) and the mid-ocean ridge axis (black lines).

[6] The modeling and inversion scheme is summarized here; details are given by *Baba and Chave* [2005] and *Baba et al.* [2006]. The analysis methodology for the northern line data is identical to that for the southern line. The computed MT responses were first corrected for topographic effects using the 3-D forward modeling method of *Baba and Seama* [2002], and then the corrected responses were inverted for a 2-D anisotropic resistivity model beneath a flat-bottomed ocean. The correction and inversion steps were iterated to check for coupling between them and it was verified that the coupling was weak, similar to the southern line [*Baba and Chave*, 2005]. The anisotropy model allows mantle resistivity (or its inverse, conductivity) to be different in the along-ridge (x), cross-ridge (y), and vertical (z) directions. In other words, the resistivity tensor is diagonal with distinct values between the diagonal elements (ρ_{xx}, ρ_{yy}, and ρ_{zz}). The inversion algorithm is an extension of the *Rodi and Mackie* [2001] non-linear conjugate gradient method that minimizes an objective function that incorporates data misfit and two regularization terms for model smoothness and degree of isotropy [*Baba et al.*, 2006].

[7] Examples of the data that were inverted and their fit to the modeled responses are shown in Figure 2. Site *f* is close to the ridge axis while site *m* is the furthest to the east. For the inversions, both the transverse electric (TE) and transverse magnetic (TM) modes were used with error floors of 10 % on the apparent resistivity and 3 % on the phase. A large number of inversions were carried out with different regularization parameters and with different a priori models. The RMS misfit decreased as the regularization parameters for the model smoothness decreased and degree of anisotropy increased, but the gradients are not constant. The optimal anisotropic resistivity model was selected from the point where the misfit is acceptable, but is away from the steepest gradients in misfit with respect to the two regularization parameters.

[8] The optimal isotropic and anisotropic models are shown in Figure 3. The RMS misfit of the anisotropic model (1.546) is smaller than that of the isotropic model (1.707) but the difference is not statistically significant. The resistive upper layer to the east of the ridge crest for the isotropic model is much thicker than that for the anisotropic model. These observations are similar to the 17°S region [*Baba et al.*, 2006]. However, unlike the result from the 17°S region, no distinct conductive region is apparent immediately beneath the ridge axis in either the isotropic or anisotropic models.

[9] The optimal model displays significant anisotropy to the east of the ridge below about 60 km depth, with a mantle that is much more conductive in the spreading direction than in the along-strike direction, similar to the 17°S region. The depth to the top of the conductive zone is independent of lithospheric age. In some models, the resistivities in the direction of plate spreading (ρ_{yy}) and in the vertical direction (ρ_{zz}) at about 15 km depth beneath the rise axis are slightly less resistive compared with the surrounding region, but this is not a required feature, and does not appear in all models. At 17°S, the mantle exhibits a triangular region of enhanced conductivity centered on the rise crest and a pipe-like conductor in ρ_{zz} immediately beneath the ridge axis [*Baba et al.*, 2006].

3. Discussions and Conclusions

[10] There is no enhanced conductivity zone immediately beneath the spreading axis in either the isotropic or anisotropic model, in contrast to the structure at 17°S. The

Table 1. Available Data From the Northern Line

Site	Distance From the Ridge Axis, km	Depth, m	Available Field Components	Combination (*E* Site/*M* Site)
d	−18.4	3122	*E*, *M*	*d*/*d*
e	−10.9	3203	*E*, *M*	*e*/*e*
f	−6.1	3026	*E*	*h*/*f*
h	6.2	3019	*M*	*h*/*f*
j	19.5	2968	*E*, *M*	*j*/*j*
k	54.7	3173	*E*	*j*/*k*
m	209.1	3673	*E*, *M*	*m*/*m*

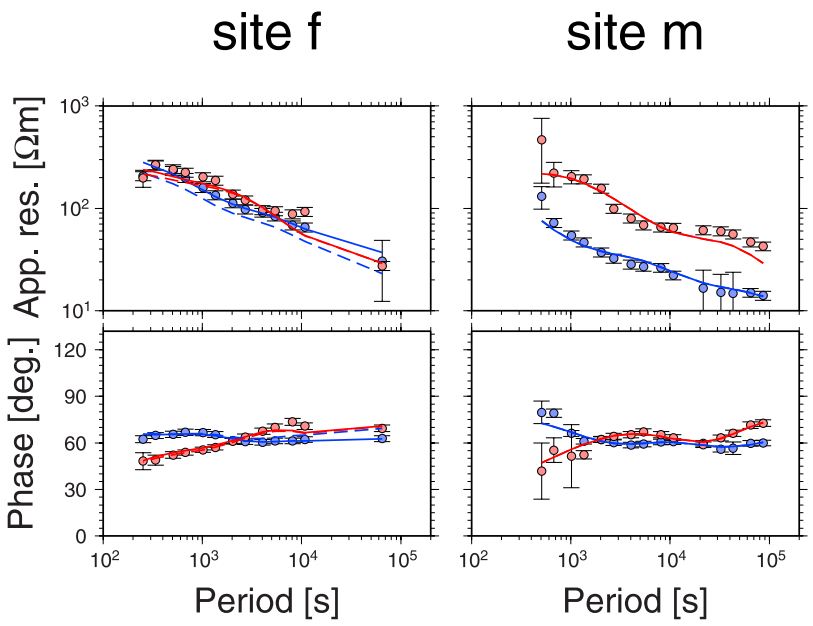

Figure 2. Examples of the MT responses applied to the inversion analysis from site *f* and *m*, which are the closet and furthest sites from the EPR ridge axis, respectively. Red and blue indicates the TE and TM modes, respectively. Solid and dashed lines are the responses calculated from the best model and the modified model for the sensitivity test shown in Figure 4.

resistivity in this region is comparable to that predicted from models of plate thermal structure and dry isotropic resistivity of peridotite based on laboratory measurements [*Xu et al.*, 2000], as calculated by *Baba et al.* [2006] (Figure 4). We have run tests to ensure that the modest density of the observation sites does not bias this observation across the ridge crest. The anisotropic resistivity model is modified to include a relatively conductive area as shown in Figure 4. The geometry of the conductive area is defined by overlapping the region for the 17°S model that is more conductive than the predicted resistivity model [*Baba et al.*, 2006, Figure 9b]. For these tests, the resistivity is replaced with 100 Ωm, which is modest compared with that observed at 17°S. The calculated responses are shown in Figure 2 as dashed lines that diverge from the optimal model response (solid lines) for sites near the ridge crest (the difference is invisible at site *m*). The RMS misfit increases to 3.291, which is significantly larger than that for the optimal model. These results indicate that the lack of a conductor is not due to poor resolution, but that indeed the resistivity directly beneath the EPR at 15°45′S is higher than that beneath at 17°S.

[11] Partial melting must have occurred beneath the EPR at 15°45′S at intervals over at least the last ∼3 Myr in order to explain the observed crustal thickness (which is at least as thick as crust at 17°S [*Canales et al.*, 1998]). Furthermore, the resistivity pattern to the east of the ridge supports the partitioning of water due to partial melting as discussed in the following paragraphs. Seafloor morphology and other geophysical observables [e.g., *Hooft et al.*, 1997] have been previously used to infer that this segment is currently magma-poor (on time scales of ∼100,000 yr). There is no suggestion of melt in the resistivity model for the region, indicating either that the melting process is episodic and currently at a nadir or that melt at 15°45′S is poorly interconnected.

[12] The anisotropy to the east of the ridge is the feature to which the data are most sensitive. In Figure 3, the sensitivity defined as log diag $(\mathbf{A}^t\mathbf{V}^{-1}\mathbf{A})$ is shown as contour lines, where $\mathbf{A}$ and $\mathbf{V}$ are the Jacobian and the error covariance matrices, respectively. The areas enclosed by larger contour values are those where the data are sensitive to small differences between the resistivities in the model blocks. The mantle between 80 and 250 km east of the ridge at 60–100 km depth in ρ_{yy} is the most prominent part.

[13] The observation of an anisotropic high conductivity zone below a depth that is independent of lithospheric age at both the 15°45′S and 17°S sites indicates that the mantle resistivity is broadly anisotropic. This resistivity pattern has been interpreted in terms of partitioning of water associated with partial melting beneath the ridge axis and strain-induced lattice preferred orientation of the mantle minerals [*Evans et al.*, 2005; *Baba et al.*, 2006]. The upper mantle is dehydrated through the partial melting process in the upper 60 km beneath the ridge axis, while the mantle below the solidus depth (∼60 km) remains hydrated [e.g., *Hirth and Kohlstedt*, 1996].

[14] Anisotropy in electrical conductivity associated with anisotropic diffusion of hydrogen in olivine has been controversial because its existence is based primarily on theoretical considerations [*Karato*, 1990; *Lizarralde et al.*, 1995]. Laboratory measurements of the conductivity of hydrous olivine have recently been conducted [*Wang et al.*, 2006; *Yoshino et al.*, 2006]. Wang et al.'s data support the interpretation that the high conductivity of ∼0.1 S/m from the MT inversions results from the presence of ∼1000 ppm H/Si in olivine. In contrast, *Yoshino et al.* conclude that hydration alone cannot explain the high conductivity below 60 km, although their experimental temperatures are significantly lower than for the asthenosphere at the depths covered by our study. Furthermore, while they observe the highest conductivity parallel to

[100] in their experiments (consistent with having a high conductivity parallel to the mantle flow direction), extrapolation of their results suggests that [100] is not the most conductive direction at high temperatures. An alternative explanation for the high conductivity and the anisotropy is a small amount of melt preferentially connected in the spreading direction, although a mechanism to explain such melt alignment is not available [*Evans et al.*, 2005].We note that if melt is present in this region of the asthenosphere, it is likely to have been induced by the presence of water. Thus it is possible that both explanations are viable and work together to enhance conductivity.

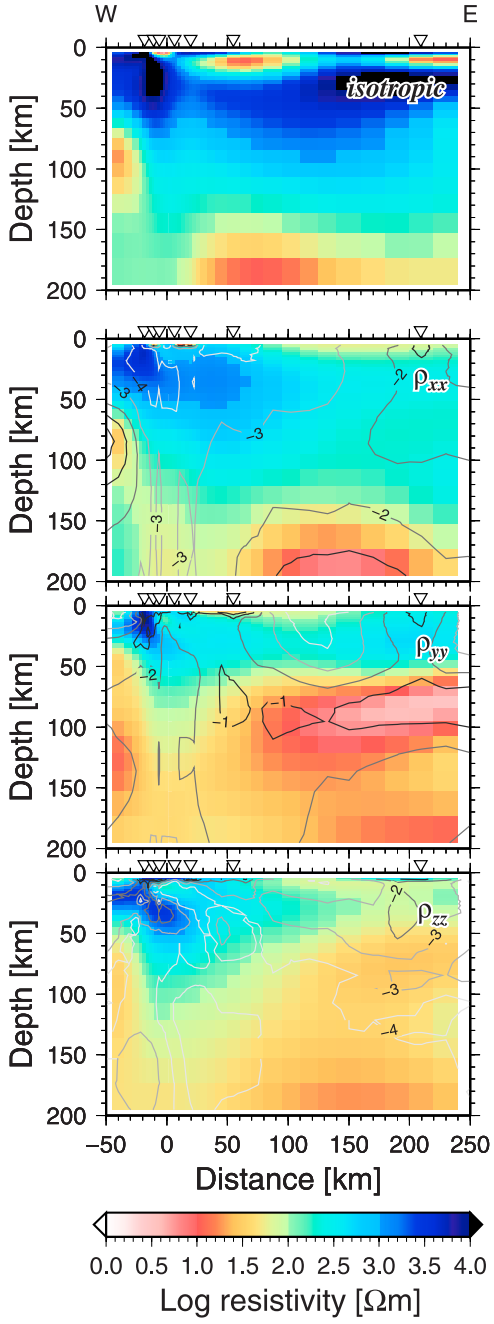

Figure 3. Optimal 2-D isotropic and anisotropic resistivity models. From top to bottom, the resistivities for the isotropic model, and the anisotropic resistivity in the along-strike, cross-strike, and vertical directions, are shown. The horizontal axis is distance from the axis of the EPR with the right side directed east. Inverted triangles indicate the location of the data used for the inversion analysis. Contour lines in the anisotropic model indicate the sensitivity of the data to the resistivity of each model block.

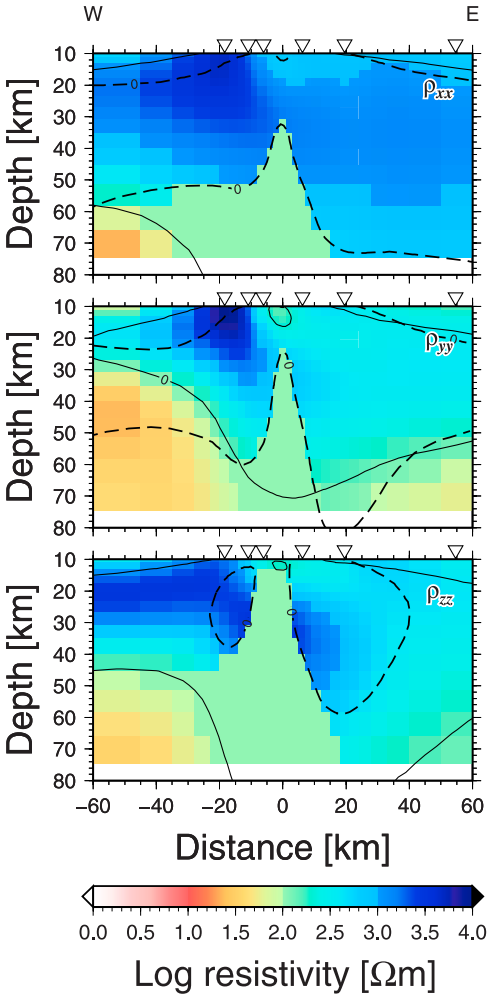

Figure 4. The resistivity model modified for a resolution test. The horizontal axis is the distance from the ridge axis. Inverted triangles indicate the locations of the observation sites. Solid lines represent that the resistivity is the same as that for a theoretical model inferred from laboratory measurements and a thermal model [*Baba et al.*, 2006, Figure 9c]. Dashed lines represent the same thing but for the resistivity model beneath the southern line (17°S).

[15] The resistive to conductive transition at a depth of around 60 km appears to be a robust feature throughout the MELT area. While we favor the idea of a dehydration boundary to explain this feature, there is still some uncertainty in this interpretation. Future work, exploring how this boundary layer evolves with lithospheric age will provide key insights into the processes of lithospheric formation. This study has demonstrated the important role that electrical conductivity measurements play in this analysis.

[16] **Acknowledgments.** The authors thank Yoshino Takashi and an anonymous reviewer for their helpful comments which improved the

manuscript. This work was supported by NSF grant OCE0118254. The inversion analyses were performed using a workstation at the Institute for Research on Earth Evolution (IFREE), Japan Agency for Marine–Earth Science and Technology (JAMSTEC). The figures were produced using the GMT software of *Wessel and Smith* [1998].

References

Baba, K., and A. D. Chave (2005), Correction of seafloor magnetotelluric data for topographic effects during inversion, *J. Geophys. Res.*, *110*, B12105, doi:10.1029/2004JB003463.

Baba, K., and N. Seama (2002), A new technique for the incorporation of seafloor topography in electromagnetic modelling, *Geophys. J. Int.*, *150*, 392–402.

Baba, K., A. D. Chave, R. L. Evans, G. Hirth, and R. L. Mackie (2006), Mantle dynamics beneath the East Pacific Rise at 17°S: Insights from the Mantle Electromagnetic and Tomography (MELT) experiment, *J. Geophys. Res.*, *111*, B02101, doi:10.1029/2004JB003598.

Canales, J. P., R. S. Detrick, S. Bazin, A. J. Harding, and J. A. Orcutt (1998), Off-axis crustal thickness across and along the East Pacific Rise within the MELT area, *Science*, *280*, 1218–1221.

Chave, A., and D. J. Thomson (2004), Bounded influence estimation of magnetotelluric response functions, *Geophys. J. Int.*, *157*, 988–1006, doi:10.1111/j.1365-246X.2004.02203.x.

Dunn, R. A., and D. W. Forsyth (2003), Imaging the transition between the region of mantle melt generation and the crustal magma chamber beneath the southern East Pacific Rise with short-period Love waves, *J. Geophys. Res.*, *108*(B7), 2352, doi:10.1029/2002JB002217.

Evans, R. L., et al. (1999), Asymmetric electrical structure in the mantle beneath the East Pacific Rise at 17°S, *Science*, *286*, 752–756.

Evans, R. L., G. Hirth, K. Baba, D. Forsyth, A. Chave, and R. Mackie (2005), Geophysical evidence from the MELT area for compositional controls on oceanic plates, *Nature*, *437*, 249–252, doi:10.1038/nature04014.

Hirth, G., and D. L. Kohlstedt (1996), Water in the oceanic upper mantle: Implications for rheology, melt extraction and the evolution of the lithosphere, *Earth Planet. Sci. Lett.*, *144*, 93–108.

Hooft, E. E. E., R. S. Detrick, and G. M. Kent (1997), Seismic structure and indicators of magma budget along the Southern East Pacific Rise, *J. Geophys. Res.*, *102*(B12), 27,319–27,340.

Karato, S. (1990), The role of hydrogen in the electrical conductivity of the upper mantle, *Nature*, *347*, 272–273.

Kurz, M. D., M. Moreira, J. Curtice, D. E. Lott III, J. J. Mahoney, and J. M. Sinton (2005), Correlated helium, neon, and melt production on the super-fast spreading East Pacific Rise near 17°S, *Earth Planet. Sci. Lett.*, *232*, 125–142, doi:10.1016/j.epsl.2005.01.005.

Lizarralde, D., A. Chave, G. Hirth, and A. Schultz (1995), Northeastern Pacific mantle conductivity profile from long-period magnetotelluric sounding using Hawaii-to-California submarine cable data, *J. Geophys. Res.*, *100*, 17,837–17,854.

MELT Seismic Team (1998), Imaging deep seismic structure beneath the mid-ocean ridge: The MELT experiment, *Science*, *280*, 1215–1218.

Rodi, W., and R. L. Mackie (2001), Nonlinear conjugate gradients algorithm for 2-D magnetotelluric inversion, *Geophysics*, *66*, 174–187.

Wang, D., M. Mookherjee, Y. Xu, and S.-I. Karato (2006), The effect of hydrogen on the electrical conductivity in olivine, *Nature*, in press.

Wessel, P., and W. H. F. Smith (1998), New, improved version of the generic mapping tools released, *Eos Trans. AGU*, *79*, 579.

Xu, Y., T. J. Shankland, and B. T. Poe (2000), Laboratory-based electrical conductivity in the Earth's mantle, *J. Geophys. Res.*, *105*, 27,865–27,875.

Yoshino, T., T. Matsuzaki, and T. Katsura (2006), Electrical conductivity of hydrous single crystal olivine: Assessment of water in the upper mantle, *Nature*, in press.

K. Baba, Earthquake Research Institute, University of Tokyo, 1-1-1, Yayoi, Bunkyo-ku, Tokyo 113-0032, Japan. (kbaba@eri.u-tokyo.ac.jp)

A. D. Chave, Department of Applied Ocean Physics and Engineering, Woods Hole Oceanographic Institution, Woods Hole, MA 02543, USA. (alan@whoi.edu)

R. L. Evans and G. Hirth, Department of Geology and Geophysics, Woods Hole Oceanographic Institution, Woods Hole, MA 02543, USA. (revans@whoi.edu; ghirth@whoi.edu)

R. L. Mackie, GSY-USA, Inc., PMB 643, 2261 Market St., San Francisco, CA 94114, USA. (randy@gsy-usa.com)

P. Tarits, IUEM, UMR 'Domaines Océaniques', Place Nicolas Copemic, F-29280 Plouzané, France. (tarits@univ-brest.fr)